Person-Specific Biophysical Modeling of Alpha-Motoneuron Pools Driven by in vivo Decoded Neural Synaptic Input

Rafael Ornelas-Kobayashi, Antonio Gogeascoechea, and Massimo Sartori

***Abstract*— Interfacing with alpha-motoneurons (MNs) is key to understand and control motor impairment and neurorehabilitation technologies. Depending on the neurophysiological condition of each individual, MN pools exhibit distinct neuro-anatomical properties and firing behaviors. Hence, the ability to assess subject-specific characteristics of MN pools is essential for unravelling the neural mechanisms and adaptations underlying motor control, both in healthy and impaired individuals. However, measuring *in vivo* the properties of complete human MN pools remains an open challenge. Therefore, this work proposes a novel approach based on decoding neural discharges from human MNs *in vivo* for driving the metaheuristic optimization of biophysically realistic MN models. First, we show that this framework provides subject-specific estimates of MN pool properties from the tibialis anterior muscle on five healthy individuals. Second, we propose a methodology to create complete pools of *in silico* MNs for each subject. Lastly, we show that neural-data driven complete *in silico* MN pools reproduce *in vivo* MN firing characteristics and muscle activation profiles during force-tracking tasks involving isometric ankle dorsiflexion, at different levels of amplitude. This approach can open new avenues for understanding human neuromechanics and, particularly, MN pool dynamics, in a person-specific way. Thereby enabling the development of personalized neurorehabilitation and motor restoring technologies.**

***Index Terms*— Neuronal modeling, optimization, high-density electromyography, motoneuron, neuromechanics.**

I. Introduction

ALPHA-MOTONEURONS (MNs) are regarded as the final common pathway of central nervous system's motor and sensory pathways. Therefore, getting insight into MN behavior *in vivo* would be key for unravelling the neural mechanisms underlying motor control, both in healthy and neurologically impaired individuals. Depending on the specific neuro-physiological characteristics of an individual, including age [1], level of training [2], [3], severity of motor disorder [4], [5] and neural injury [6], pools of MNs exhibit distinctive neuro-anatomical properties and dynamics. For this reason, the ability to assess subject-specific MN pool characteristics is essential to understand motor impairment and enable the development of tailored neurorehabilitation technologies.

Signal-based approaches relying on high-density electromyography (HD-EMG) decomposition [7], [8], [9] enable identifying the firing output of MNs *in vivo* [10], [11]. These allowed the estimation of motor unit properties as innervation zone and conduction velocity of muscle fibers [8]. However, there is currently no existing method for characterizing the electrophysiological properties of complete MN pools *in vivo*.

In this context, biophysical models based on Hodgkin and Huxley's description [12] enable establishing a link between a neuron's firing response to an arbitrary input and its electrophysiological properties (*i.e.,* membrane resistance, capacitance, voltage threshold, conductance of ionic channels, etc.). Previous implementations of biophysical MN models in motor control [13], [14] investigated the neural mechanisms of force steadiness [15], postural balance [16] and voluntary movement [17], suggesting that a pool of MNs receive a common synaptic input (CSI) that is linearly transformed into the neural drive to muscle [17]. However, these computational approaches relied on neuronal data derived from animal preparations [18], [19]. As such, current models are not able to capture electrophysiological differences among human individuals, nor to reproduce experimental firing patterns of human MNs *in vivo* during the execution of a motor task, thus limiting the clinical implications of these findings.

Metaheuristic optimization [20], [21] has been proposed for identifying neuron model parameters that reproduce experimental spike trains, including ionic properties of cortical interneurons [22] and cerebellar granular neurons [23]. Despite successfully characterizing neuron dynamics, these methods have only been implemented *in vitro*, where firing responses to controlled input currents injected into the soma can be recorded.

This work proposes merging HD-EMG decomposition, biophysical modelling and metaheuristic optimization to create

Manuscript received 21 July 2022; revised 24 November 2022 and 16 January 2023; accepted 26 January 2023. Date of publication 22 February 2023; date of current version 6 March 2023. This work was supported by the European Research Council (ERC) under the European Union's Horizon 2020 Research and Innovation Program as part of the ERC Starting INTERACT under Grant 803035. *(Corresponding author: Rafael Ornelas-Kobayashi.)*

This work involved human subjects in its research. Approval of all ethical and experimental procedures and protocols was granted by the Medical Ethical Committee at Radboudumc, under Research Protocol NL73230.091.20.

The authors are with the Department of Biomechanical Engineering, University of Twente, 7522 NB Enschede, The Netherlands (e-mail: r.e.ornelaskobayashi@utwente.nl; a.d.j.gogeascoecheahernandez@utwente.nl; m.sartori@utwente.nl).

Digital Object Identifier 10.1109/TNSRE.2023.3247873

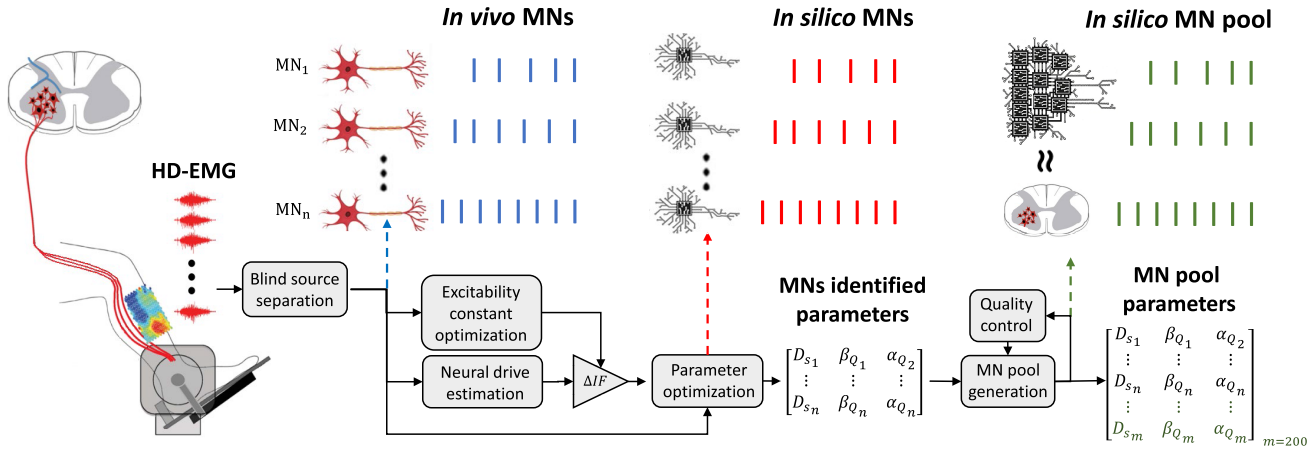

Fig. 1. Overview of neural-data driven framework for generating *in silico* motoneuron (MN) pools: *in vivo* spike trains are decoded from high-density electromyography recordings via convolution kernel compensation blind source separation decomposition [9]. A subject-specific excitability constant (ΔIF) is determined using multiple objective optimization, and the common synaptic input (CSI) received by the MN pool is computed as the product of ΔIF and the neural drive derived from *in vivo* MNs. Parameter optimization of *in silico* MNs driven by the CSI is then performed to minimize recruitment time error and frequency-corrected temporal spike match. Based on probability density functions of the identified parameters, additional *in silico* MNs are generated to complete an *in silico* pool of 200 MNs.

a novel neural-data driven framework. This approach consists of decoding the activity of human MNs *in vivo* via HD-EMG decomposition, and using it to drive the metaheuristic optimization of biophysically realistic MN models. The outcome are physiologically realistic estimates of complete MN pool properties (*i.e.* distributions of soma sizes, ionic channel dynamics, pool excitability) from specific subject's muscles, which subsequently enable the creation of *in silico* MN pools that retain the same statistical behavior of their *in vivo* counterparts. Our results evidence the ability of this method for predicting *in vivo* MN firing characteristics and muscle activation profiles throughout isometric force-tracking tasks at varying levels of amplitude from the tibialis anterior (TA) muscle on a group of five healthy individuals.

This approach opens new avenues for understanding the neuronal mechanisms underlying human movement in a person-specific way, thereby bridging the gap limiting the development of personalized neurorehabilitation therapies and motor restoring technologies.

II. Methods

This framework consists of three main components (Fig. 1): 1) approximation of *in vivo* CSI from HD-EMG decomposed MN spike trains, 2) parameter optimization of *in silico* MN models driven by *in vivo* CSI to match recruitment time and firing frequency of *in vivo* MNs, 3) generation of extended *in silico* MN pools following subject-specific experimental distributions of biophysical properties. These steps will be described along study procedures from section II-C. onwards.

A. Participants Overview

Five healthy subjects were recruited (age: 27.4 ± 2.07 years, weight: 70 ± 12.34 kg, height: 173.6 ± 10.06 cm), who provided a written informed consent to participate in this experiment. All procedures were executed in compliance with the medical ethical committee at Radboudumc, under the research protocol NL73230.091.20.

B. Experimental Setup

After localization of TA's muscle belly via palpation, the skin was shaved and lightly abraded using abrasive paste (Meditec,Pharma). An 8 × 8 electrode grid with conductive gel was placed as described previously [24]. Subjects seated on a Biodex chair (M4 Biodex Medical Systems Inc., Shirley, NY, USA), with the right leg fixed with a knee joint angle of 140° flexion and the right foot tightly strapped to the dynamometer keeping the ankle joint angle in a neutral position. Isometric ankle dorsi-flexion torque was acquired at a sampling frequency of 512 Hz using National Instruments Data Acquisition card (NI DAQ), while HD-EMG data was simultaneously recorded via an in-house developed data acquisition interface using TMSi Refa multichannel amplifier (TMS International B. V., Oldenzaal, The Netherlands) at a sampling frequency of 2048 Hz.

To determine the maximum voluntary contraction (MVC), subjects were asked to apply maximal dorsi-flexion force for a period of 5 s. This was repeated three times, with a resting time of 1 min between each trial.

C. Study Protocol

Subjects performed a ramp-and-hold task at five different target % MVC amplitudes: 10, 20, 30, 40, and 50% MVC. The holding period of the ramp was set to 5s, and the speed of the ascending-descending portions was set to 20% MVC/s.

Throughout the experiment, all five target %MVCs were sorted randomly and five consecutive repetitions, for each amplitude, were presented to the subjects through a visual interface providing real-time feedback of the force-tracking performance. To avoid the effects of fatigue, subjects had a resting time of 5, 10, 15, 20 or 25s between each of the five repetitions, depending on if the current target %MVC amplitude was 10, 20, 30, 40 or 50%, respectively. Additionally, there was a 120s resting period between the end of the five repetitions and the next target %MVC amplitude.

Prior to recording, subjects underwent a learning trial to familiarize with the force-tracking task: two repetitions for

each target %MVC presented randomly with the same resting rules.

D. High-Density Electromyography Decomposition

HD-EMGs were band-pass filtered with a 20 to 500 Hz zero-phase Butterworth filter, and decomposed into individual spike trains using convolution kernel compensation blind source separation [9]. Each decomposed experimental spike train was as a binary vector where '1' represented a spike event and '0' meant no firing activity. Decomposed spike trains underwent a quality-control algorithm (QC-MN), as previously proposed [24], to ensure pulse-to-noise ratio (PNR) $>$ 20 dB, coefficient of variation $<$ 0.3, and discharge rates $<$ 30 Hz [24]. These thresholds were chosen to remove non-physiological spike trains while keeping a significative amount per trial. MNs not fulfilling this criterion were excluded.

E. Biophysical Motoneuron Model

MNs were described as single-compartment conductance-based models including leakage (g_l) sodium (g_{Na}), slow (g_{Ks}) and fast potassium (g_{Kf}) channels, which have been identified to reflect experimental neuronal behavior [13]. Ionic current was determined according to (1), where E_{Na} and E_K correspond to the reverse potentials of sodium and potassium, respectively. Voltage-dependent rate constants (m, h, n, q) were computed using a pulse-based model [25], which describes action potentials as rectangular pulses and defines each rate constant based on parameters beta (β_i) and alpha (α_i), where subscript i denotes each rate constant [25].

MN's leakage conductance (2) and capacitance (C) (3) were adjusted by the soma diameter (D_s), where R_m and C_{m} are membrane specific resistance and capacitance, respectively. Membrane voltage (V_m) was then computed according to (4), where E_L represents leakage Nernst voltage and I_{inj} the current injected in the soma.

$$I_{ion} = g_{Na} m^3 h\,(E_{Na} - V_m) + g_{Kf} n^4\,(E_K - V_m) + g_{Ks} q^2\,(E_K - V_m) \tag{1}$$

$$g_l = \frac{\pi D_s^2}{R_m} \tag{2}$$

$$C = \pi C_m D_s^2 \tag{3}$$

$$V_m = \left(g_l\,(E_L - V_m) + I_{ion} + I_{inj}\right)\left(\frac{dt}{C}\right) \tag{4}$$

F. Common Synaptic Input Estimation

The *in vivo* CSI current (in pA) was computed as the product between the net discharge rate of the MN pool (in Hertz) and a subject-specific gain (ΔIF). This way, *in vivo* CSIs enabled recruiting *in silico* MNs in a range of D_s matching experimental measurements (*i.e.,* $15 < D_s < 220$ μm) [26]. The net discharge rate of the MN pool (*i.e.,* neural drive) was derived as the low-pass filtered sum of trial-specific MN spike trains (*i.e.,* cumulative spike train filtered by 200 ms Hann window) [17], normalized by the average discharge rate of summated MNs. ΔIF was determined via multi-objective optimization of recruitment error (5) in two conditions: a) earliest recruited *in vivo* MN and *in silico* MN with lowest soma diameter, and b) latest recruited *in vivo* MN and *in silico* MN with highest soma diameter. All remaining parameters were kept as previously proposed [14], since prior work [27] demonstrated dominance of D_s over recruitment time. Optimization was executed using MATLAB's genetic algorithm (The MathWorks, Inc., Natick, MA, USA) for a Gaussian distributed initial population size of 200 ΔIFs in the range of 0.1 to 1, an elite percentage of 10%, 70% cross-over, and a function tolerance of 0.01. Gray relational analysis [28] was subsequently applied on the resulting pareto set to automatically determine the ΔIF that best minimized both error functions. This process was performed on every participant, and each subject-specific ΔIF was kept constant throughout the entire study.

G. Motoneuron Parameters Identification

MN parameter identification was performed on one trial per target %MVC (Section II-B), which yielded the highest number of decomposed MNs. The remaining trials were kept for validation of force-profile tracking *in silico* MNs (Section II-I).

in silico MN models were created and paired to each *in vivo* decomposed MN. Subsequently, the *in silico* MNs were driven by the CSI derived from each corresponding target % MVC trial (see section II-F). We implemented a double single-objective optimization approach for robust sampling of the optimal pareto space without increasing computational load [29]. First, relative recruitment error (5) between *in silico* and *in vivo* MNs was minimized by optimizing D_s within the anatomical range of 15 to 220μm [26]. Subsequently, spike-match (*i.e.* gamma-factor [30]) error (6), was minimized by the optimization of β_Q and α_Q, as early work [27] indicated slow-potassium dynamics to largely determine MNs' firing features.

$$2\left|\frac{spikes_e(i) - spikes_m(i)}{spikes_e(i)}\right|_{i=1} \tag{5}$$

$$2\left|\frac{f_e - f_m}{f_e}\right| - \frac{2}{1 - 2\delta f_e}\left(\frac{N_c - 2\delta f_e N_e}{N_e + N_m}\right) \tag{6}$$

where f_e and f_m represent the mean firing rate, N_e and N_m the number of spike events, and $spikes_e$ and $spikes_m$ the spike trains of experimental (i.e. *in vivo)* and model (i.e. *in silico)* MNs, respectively. N_c is the number of coincident spikes within the time window $\delta = 2$ms [30].

Optimization of both objective functions implemented MATLAB's genetic algorithm set to a population size of 200, elite percentage of 20%, cross-over of 70%, and function tolerance of $1e^{-5}$. Furthermore, the initial populations for every parameter were generated randomly with uniform distributions. To constrain the framework for providing physiologically realistic solutions, the lower and upper boundaries of β_Q and α_Q, as well as non-optimized parameters of the model were kept the same as proposed previously [14].

After optimization, identified sets of MN parameters from all %MVC amplitudes were merged together, and the probability density function (PDF) of each parameter was computed using boundary-corrected kernel density estimator [31].

H. Generation of Complete in Silico Motoneuron Pools

As indicated by Duchateau and Enoka [32], MN pool size estimations of TA taken from human cadavers (i.e., 445 MNs) may be overestimated, as electrophysiological approaches [33] indicate a mean size of 200 ± 61 MNs. Since the usual number of identifiable MNs via HD-EMG decomposition is limited to few tens of MNs at forces up to 50% [7], [8] and 70% MVC [3], additional *in silico* MNs based on subject-specific parameter's PDFs were generated to create customized pools of 200 MNs for every participant. First, D_s values were randomly generated from the corresponding PDF. Following previously proposed size-based ranges of β_Q and α_Q for different MN-types [14], k-means clustering [34] was subsequently performed to identify three clusters of parameters, thereby defining cluster-specific PDFs. For each generated D_s, the corresponding cluster *was* identified computing the minimal distance to their centroids, and the values of β_Q and α_Q were generated according to the cluster-specific PDF.

PDF-derived *in silico* MN underwent a pool quality-control algorithm to exclude sets of parameters resulting in unrealistic discharge rates (*i.e.,* $f_m > \max(f_e) + 3\text{Hz}$). This consisted of iterative simulations of MNs driven by the CSI derived from the highest %MVC amplitude (*i.e.,* where higher discharge rates can be found). For each iteration, PDF-derived *in silico* MNs not fulfilling discharge rate criteria were considered non-realistic and discarded, the rest were approved and kept in the pool. New sets of MN parameters were created following the same rules, and the same procedure was repeated until all *in silico* MNs in the pool fulfilled the discharge rate constrain.

I. Force-Tracking in Silico Motoneuron Pools

The relation between force produced by TA's motor units and the percentage of recruited MNs in the pool has been described by an exponential fit [32]. As the force required to reach 100% MN recruitment in TA is reportedly decreased at high rates of force development (*i.e.,* from ∼90% to ∼50% MVC) [35], [36] we modified the fit function [32] accordingly (7) and implemented it to control the percentage of MN recruitment as a function of % MVC throughout our simulations.

$$Recruited\ MNs[\%] = \frac{log\,|MVC|}{0.0389} - 2.118 \qquad (7)$$

J. Validation Procedures

Test 1 assessed whether optimization of proposed objective functions enabled finding unique solutions for creating *in silico* MN copies that fire similarly to *in vivo* MNs. For this, we quantified the costs values of objective functions (5) and (6) before optimization (*i.e.* using a set of initial parameters $\left[D_{s_0}, \beta_{Q_0}, \alpha_{Q_0}\right] = [30, 0.03, 1.5]$ corresponding to an average small size MN, reportedly dominant in TA [37] and traditionally associated to slow-type motor units [14]), and after optimization. Additionally, we tested the repeatability of the solutions on a representative set of 20 *in vivo* MNs derived from a 50% MVC trial (*i.e.,* including MNs from all recruitment thresholds). For each MN, we performed ten consecutive optimizations and measured the standard deviation (STD) of the resulting parameters.

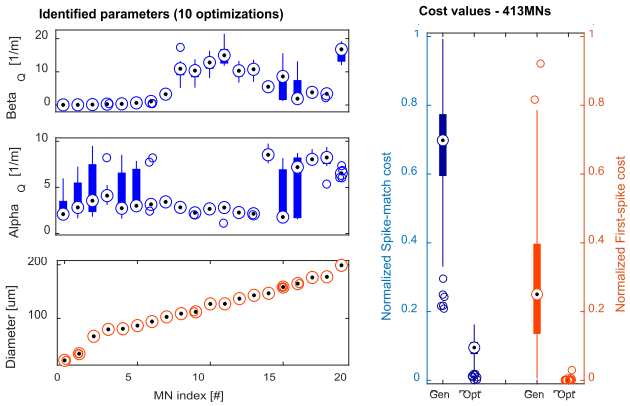

Fig. 2. Left panel: Identified parameters for a set of 20 representative motoneurons (MNs) after 10 consecutive optimizations. Parameters depicted in blue correspond to minimization of spike-match cost, Orange corresponds to minimization of first-spike cost. Right panel: Cost values of spike-match (blue) and first-spike (orange) for all *in silico* MNs before (Gen) and after optimization (Opt). Plots normalized by the respective maximum cost of each objective function.

Test 2 evaluated inter-subject variability in the identified MNs PDFs. Assessed metrics included mean and STD among MN parameters and cluster thresholds.

To validate whether *in silico* MNs driven by a trial-specific CSI produced firing outputs of similar characteristics as their *in vivo* counterparts, test 3 quantified absolute error in recruitment time and mean discharge rate (during plateau) between *in vivo* and *in silico* MNs. This was performed on two conditions: before and after parameter optimization.

Test 4 assessed the ability for creating extended *in silico* MN pools from subject-specific parameter's PDFs. This analysis included quantification at intra-subject level of median and STD, as well as visual PDF inspection, of the parameters describing optimized *in silico* MNs (*i.e.,* the total number of decomposed MNs) and extended *in silico* pools including PDF-derived *in silico* MNs (*i.e.,* 200 MNs).

Test 5 evaluated whether the use of extended *in silico* MN pools driven by trial-specific CSIs improved the estimates of force profiles (*i.e.,* neural drive) throughout all conditions. Two metrics were used for this: 1) Coefficient of determination (R^2) between measured torque and neural drive. 2) Coefficient of variation (CoV) of neural drive. Statistical differences between R^2 and CoV of *in vivo* MNs, their corresponding *in silico* copies, and the extended *in silico* MN pool (including PDF-derived *in silico* MNs) were tested using non-parametric Friedman test.

III. Results

After HD-EMG decomposition and QC-MN, a total of 413 MNs (PNR = 31.11 ± 7.2) from all subjects and conditions were included in the study. MN count per subject is shown in Fig. 3.

For all participants, the determined ΔIF values were similar (Table I), with an inter-subject mean $\Delta IF = 2.049 \pm 0.195\ \frac{Hz}{pA}$.

Test 1: After optimization, normalized cost values of both objective functions (5) and (6) decreased by one order of

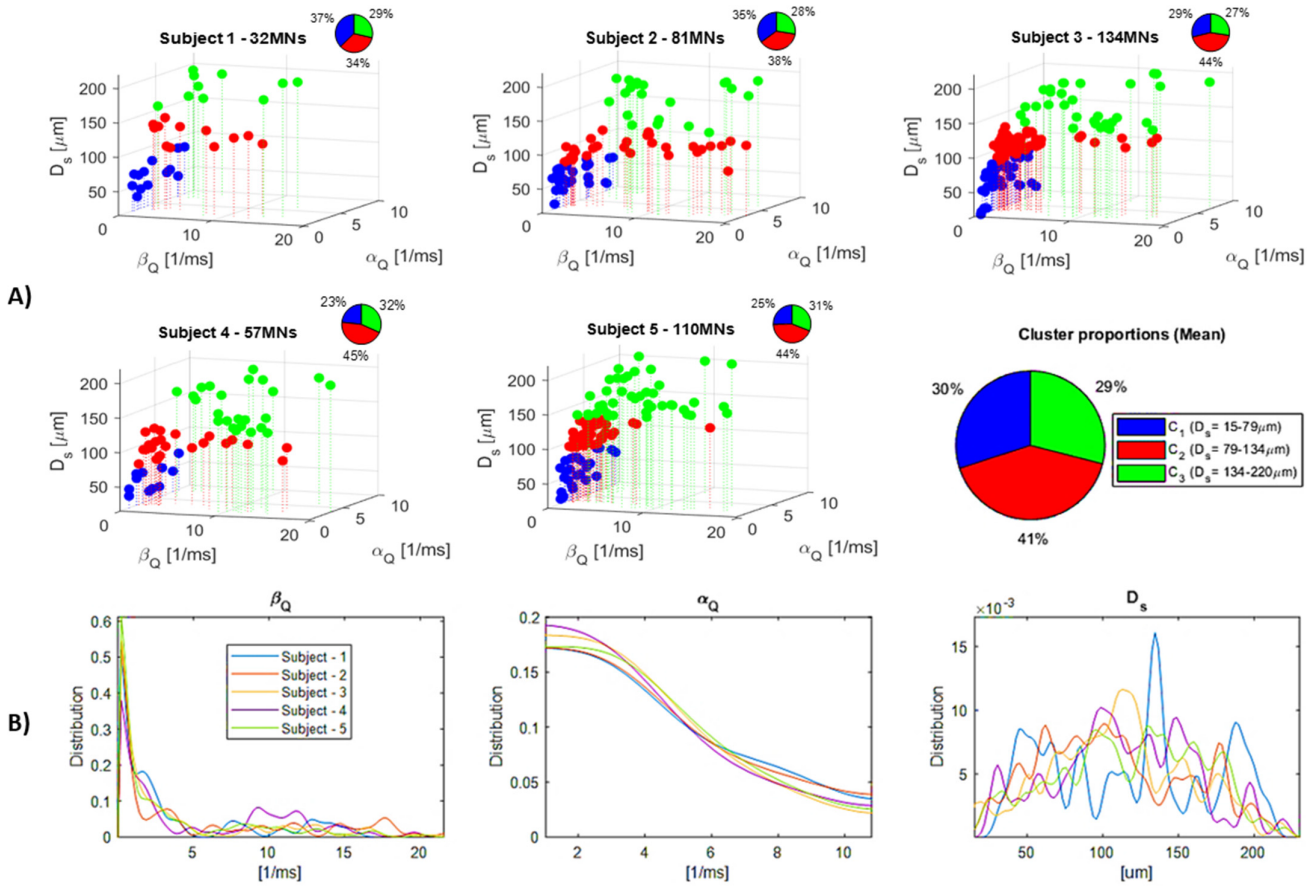

Fig. 3. Subject-specific *in vivo* motoneuron (MN) properties identified by the optimization framework. Each MN is described by three parameters: beta (β_Q), alpha (α_Q) and soma diameter (D_S). A) K-means clustering consistently identified three clusters of parameters across all subject. These clusters were characterized for having a diameter threshold of $D_S = 79.44 \pm 5.28$ μm between C_1 and C_2, and $D_S = 133.88 \pm 2.54$ μm between C_2 and C_3. The three clusters are color-coded in blue, red and green, corresponding to C_1, C_2 and C_3. Additionally, the percentage of each cluster within the MN pool is depicted on the upper right corner of each subject's specific parameter characterization. Lastly, we show a pie chart depicting the averaged cluster proportions and D_S threshold from all subjects. B) Each column shows the subject-specific distribution found for each MN parameter.

TABLE I
SUBJECT-SPECIFIC EXCITABILITY CONSTANTS (ΔIF)$\left[\frac{Hz}{nA}\right]$

Subject [#]	1	2	3	4	5
ΔIF $\left[\frac{Hz}{nA}\right]$	2.05	2.24	1.95	2.23	1.78

magnitude for all subjects (Fig. 2). For the recruitment time error function (5), cost values approached zero in all cases. Repeatability test (Fig. 2) showed no difference in estimated D_s for any MN after consecutive optimizations (average STD = 0.018). For β_Q and α_Q, the average STDs were 1.511 and 1.212, respectively.

Test 2: The inter-subject mean value of D_S was 113.53 $\pm$ 5.2 μm. Throughout all subjects, three clusters (C_i) of MN parameters were identified (Fig 3.A), with both β_Q and α_Q showing increasing amplitude and spread as D_s increases. All five subjects showed D_s thresholds separating three clusters of parameters. The inter-subject threshold between C_1 and C_2 was found at $D_s = 79.44 \pm 5.28$ μm, whereas the threshold between C_2 and C_3 was $D_s = 133.88 \pm 2.54$ μm. Based on to these cluster thresholds, the proportions of MN sizes found in the pool included: $C_1 = 28.6 \pm 5.59\%$, $C_2 = 39.6 \pm 4.72\%$, and $C_3 = 31 \pm 4.85\%$ (Fig. 3.B). Similarities in inter-subject PDFs were found for the three MN parameters (Fig. 3.C), with the largest differences found in D_s, where seemingly multi-modal distributions can be observed.

Test 3: Fig. 4 shows a representative instance of the spike trains produced by *in silico* MNs (from subject 2) before and after optimization. Recruitment time of *in silico* MNs before optimization remained unaltered for all cases (Fig. 4.A), and the net discharge rate exhibited a limited range that varied from 6.78 to 7.42 Hz as %MVC increased (Fig. 4.C). In contrast, *in silico* MNs after optimization matched recruitment time of *in vivo* MNs with an error of < 0.01 s (Fig. 4.B), and enabled replicating the full experimental net discharge rate range of 9.45 to 14.69 Hz (Fig. 4.C). The firing characteristics of identified *in vivo* MNs and their *in silico* counterparts (before and after optimization) from all trials are depicted per subject in Fig. 5. As shown by the boxplots in Fig. 6, the absolute errors in recruitment time and mean firing frequency (during plateau) were significantly reduced across all conditions after parameter optimization: the absolute recruitment time error median decreased from 365.7 ms to 0.48 ms, and the maximum outlier value from 2.69 s to 0.017 s. For absolute discharge rate error, optimization decreased the median value

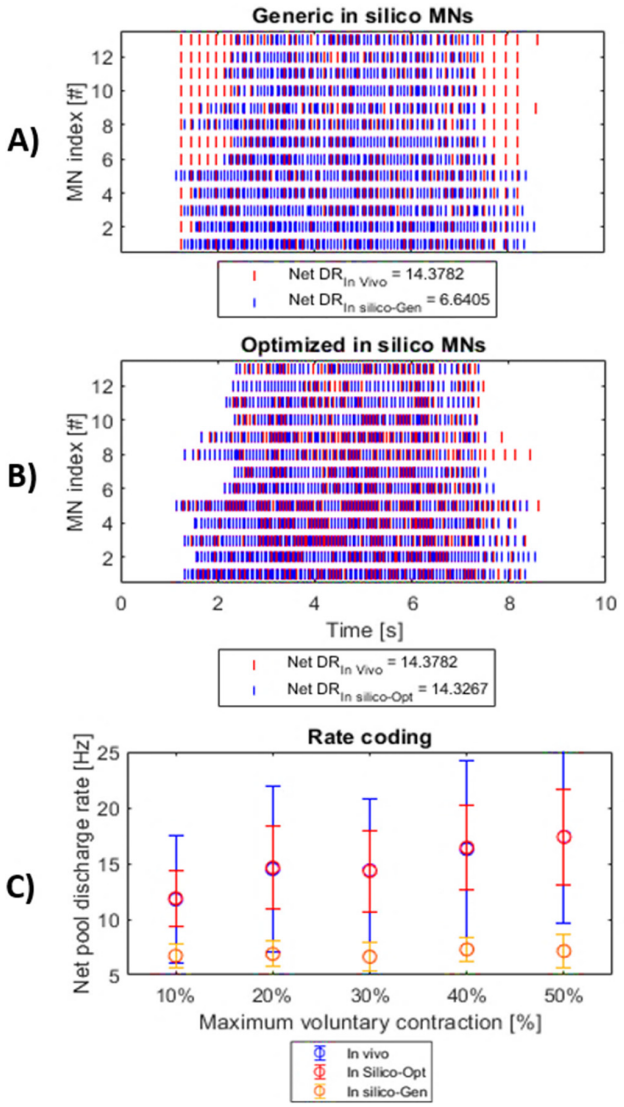

Fig. 4. Example of *in silico* MNs spike trains and estimated net discharge rate of the MN pool, before (*i.e.,* generic) and after (*i.e.,* optimized) parameter optimization (subject 2). A) *in vivo* (blue) and generic *in silico* (red) MN spike trains. B) Optimized *in silico* MN spike trains (red) (matching *in vivo* MNs (blue). C) Estimated net discharge rate of MNs (*i.e.,* low pass filtered cumulative spike train, normalized by average discharge rate of all MNs) for each % MVC amplitude using spike trains from *in vivo* (blue), generic *in silico* (orange) and optimized *in silico* (red) MNs.Error bars depict standard deviation.

from 5.8858 Hz to of 0.208 Hz, and the maximum outlier from 13.86 HZ to 5.75 Hz.

Test 4: Our proposed algorithm for extending the number of *in silico* MNs to complete a pool size of 200 MNs did not alter the original parameter's PDFs (Fig. 7). This held true regardless of the number of *in vivo* MNs identified for each subject (*e.g.,* for subjects one and four, only 18% and 30% of the MNs in the pool were identified, respectively, whereas 64% was identified for subject three). In all cases, the PDFs remained largely unaltered. There were no considerable differences in the median or STD of the subject-specific PDFs of the extended *in silico* MN pools (Table II).

Test 5: Fig. 8 shows an example of a subject-specific *in silico* MN pool (from subject four) driven by the CSI corresponding to each target %MVC amplitude. As depicted by the raster plots (Fig. 8.A) showing the firing activity of the *in silico* MNs, the percentage of pool recruitment increased logarithmically as torque increased, going from ∼60% recruitment at 10 % MVC, to ∼100% recruitment at 50%MVC. For all %MVC amplitudes (Fig. 8.B), the neural drive produced by the *in silico* MN pool closely resembled the corresponding force profile, achieving an $R^2 = 0.86 \pm 0.04$ with p-values < 0.005, and CoV $= 68.12 \pm 7\%$. In contrast, the neural drive estimated from *in vivo* MNs (Fig. 8.C) resulted in $R^2 = 0.723 \pm 0.08$ and CoV $= 75.47 \pm 11.78\%$. Fig. 9 shows R^2 and CoV of *in vivo* MNs, optimized *in silico* MNs, and extended *in silico* pool across all subjects and conditions. The non-parametric Friedman test showed no significant difference in either R^2 or CoV between *in vivo* and *in silico* MNs, indicating that *in silico* MN pools generated through this framework closely mimic the firing characteristics of their *in vivo* counterparts. Between *in vivo* MNs and extended *in silico* pool, however, non-parametric Friedman test showed statistically significant improvement in R^2, which increased from 0.7997 ± 0.08 to 0.8716 ± 0.06. This represents a relative improvement of $9.66 \pm 7.41\%$ using the *in silico* MN pool, in comparison to only *in vivo* MNs. Although not statistically significant, the CoV corresponding to the extended *in silico* pool decreased relatively to the *in vivo* MNs by 5.16 ± 4.49 %.

IV. Discussion

This work combined HD-EMG decomposition, biophysical neuronal modelling and metaheuristic optimization to characterize the subject-specific physiological properties of complete pools of MNs innervating TA in healthy individuals. For this, we established *in silico* MN models driven by *in vivo*-derived CSI, and optimized their parameters to reproduce the firing behavior of *in vivo* MNs. Subsequently, we used PDFs from the identified parameters as blueprints to create complete subject-specific *in silico* MN pools capable of estimating MN pool activity and muscle activation profiles for TA throughout multiple levels of isometric activation.

The excitability of a single MN is described by its current-frequency slope [38]. Analogously, here we proposed ΔIF as the slope between CSI and the net firing activity of the MN pool. Hence, ΔIF can be interpreted as a subject-specific parameter reflecting spinal excitability. We found relatively similar values of ΔIF for all subjects (table I). This may be due to the inclusion of only healthy subjects from a population of similar ages and sizes. Notably, the identified values of ΔIF matched with experimental current-frequency slopes reported for single MNs (1.7556 ± 0.4953 $\frac{\text{Hz}}{\text{pA}}$) in the primary firing range (<40 Hz) [38]. Additional studies are required to assess whether ΔIF may reflect the averaged current-frequency slopes of single MNs within the pool.

As this framework relies on the availability of *in vivo* MNs representing the entire pool, the experimental protocol is key to ensure the activation of different types of motor units. Here, we used trapezoidal ramps at a constant rate of force development where target forces were reached in $0.5 < t < 2.5$ s. Evidence of decreased recruitment thresholds in TA's

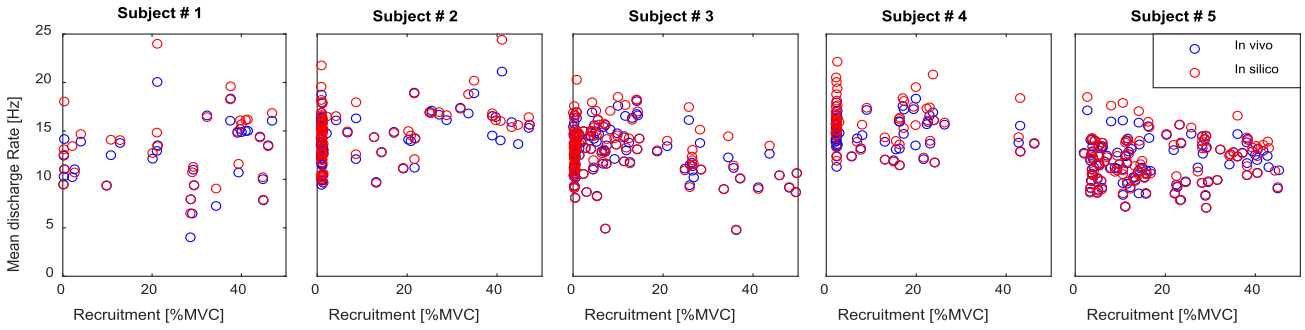

Fig. 5. Mean discharge rate at plateau vs recruitment threshold of *in vivo* (blue) and optimized *in silico* (red) motoneurons throughout all trials.

TABLE II
SUBJECT-SPECIFIC BIOPHYSICAL PROPERTIES OF *in Vivo* IDENTIFIED MNS AND *in Silico* POOLS 200 MNS (MEDIAN ± STD)

Subject [#]	Ds [um]		β_Q [Hz/s]		α_Q [Hz/s]	
	Identified	Pool	Identified	Pool	Identified	Pool
1	129.24 ± 53.68	129.19 ± 49.35	1.64 ± 4.91	1.755 ± 4.63	3.33 ± 2.37	3.09 ± 2.28
2	102.10 ± 49.17	101.92 ±46.11	2.60 ± 6.56	2.25 ± 6.45	3.37 ± 2.40	3.42 ± 2.43
3	109.76 ± 44.83	113.51 ± 44.61	1.26 ± 5.47	1.48 ± 5.31	3.25 ± 2.05	3.35 ± 2.06
4	110.97 ± 45.65	106.26 ± 43.78	2.31 ± 5.53	2.12 ± 5.11	3.15 ± 2.25	3.26 ± 2.01
5	122.80 ± 47.46	125.49 ± 46.55	1.22 ± 4.76	1.40± 4.72	3.27 ± 2.09	3.34 ± 2.18

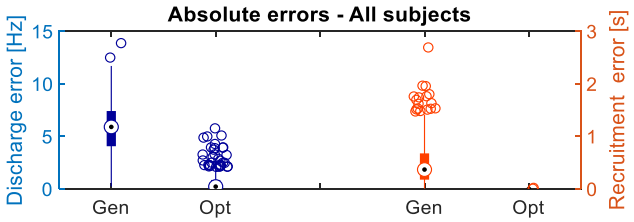

Fig. 6. Absolute error in mean discharge rate [Hz] and recruitment time [s] between *in vivo* MNs and *in silico* MNs before (Gen) and after parameter optimization (Opt) across all subjects and conditions.

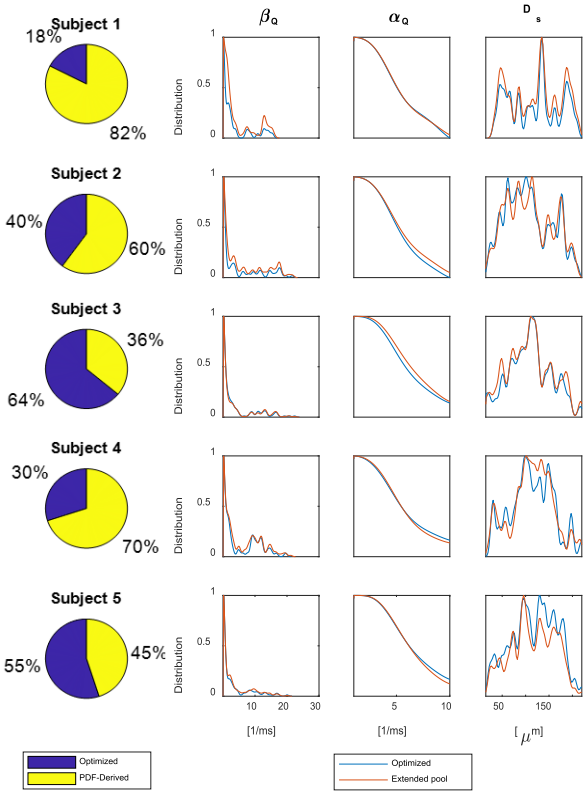

Fig. 7. Proportion of optimized (blue) and PDF-derived (yellow) *in silico* MNs for every subject (left). Parameter distributions of optimized MNs (blue) and extended *in silico* pools of 200MNs (orange) (right) show that identified parameter distributions remain unaltered in the *in silico* pool.

MNs at this rates [35] suggests that MNs from all thresholds of recruitment could be activated for the levels of forces included in this study [39]. However, HD-EMG decomposition does not guarantee the identification of every MN, particularly from deeper motor units or in the upper/lower end of recruitment order. Due to the importance of the latter for estimating ΔIF, not identified MNs of the earliest/latest recruitment order in the muscle may lead to over/under estimated ΔIFs, respectively. Additional studies are necessary to assess the impact that this may have over the resulting parameter's PDFs.

In agreement with Henneman's size principle [40], we found that optimization of D_S substantially minimized recruitment error (5) (Fig. 2), evidencing the key role of MN soma size over recruitment order. Spike-match (6), minimized through optimization of β_Q and α_Q, yielded relatively larger cost values in comparison. This may be due to the short time window used for determining coincident spikes ($\delta = 2$ms), as well as the exclusion of other ionic channels. Spike-match could be further enhanced by optimizing additional ionic channel properties, thought it would increase computational load and parameter space. In terms of repeatability, D_S showed neglectable variability throughout repeated optimizations (Fig. 2). This is not the same for β_Q and α_Q, which can be explained by the intrinsic randomness behind temporal MN firing patterns and metaheuristic optimization. However, although both parameters showed variability across repeated optimizations, each oscillated around a mean value seemingly related to D_S. As shown in Fig. 3, we found that value and spread of β_Q and α_Q increased with D_S, suggesting proportionality be between voltage-dependent rates and MN soma size.

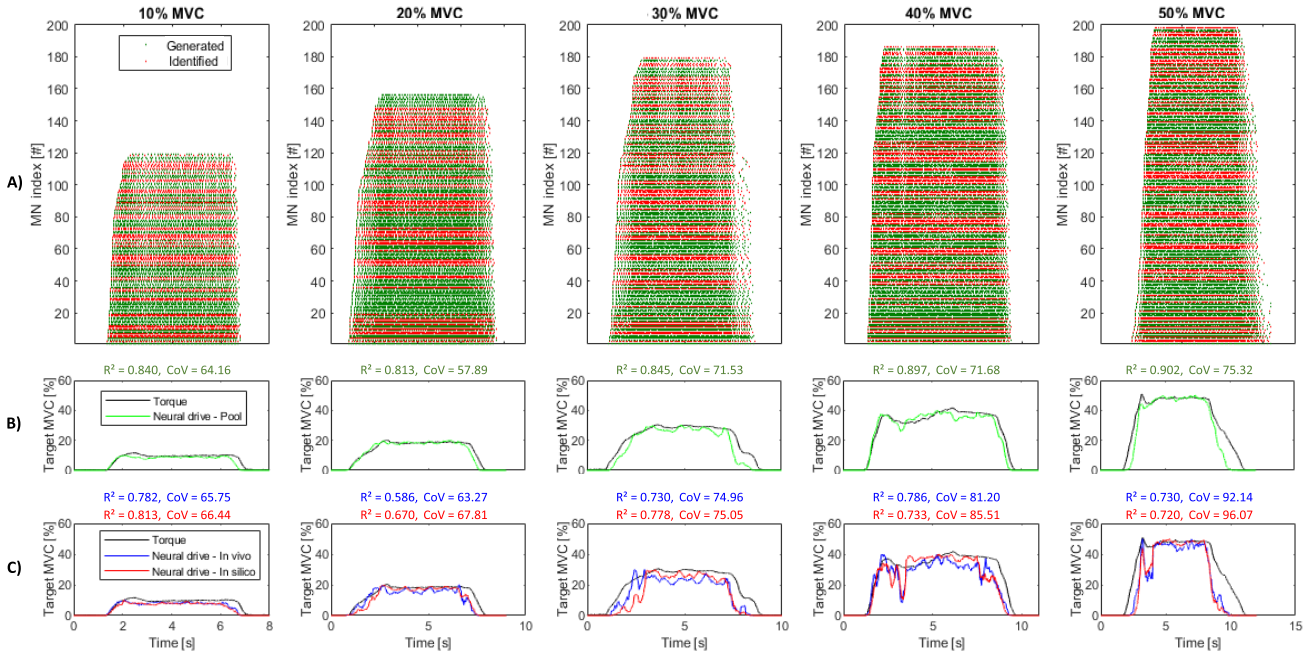

Fig. 8. Example of firing activity and force profiles produced by the *in silico* MN pool (from subject 4) for all levels of % MVC amplitude. A) The raster plots shows optimized *in silico* MNs (red) and the PDF-derived MNs (green) sorted in ascending order by diameter size. B) The measured torque (black) and neural drive produced by *in silico* MN pool (green) are plot together. On top of each figure, the coefficient of variation (CoV) and determination (R^2) are depicted (green). C) Measured torque is plot together with the neural drive derived from *in vivo* decoded (blue) and optimized *in silico* MNs (red). In accordance with this same color code, CoV and R^2 are shown for on top of each figure.

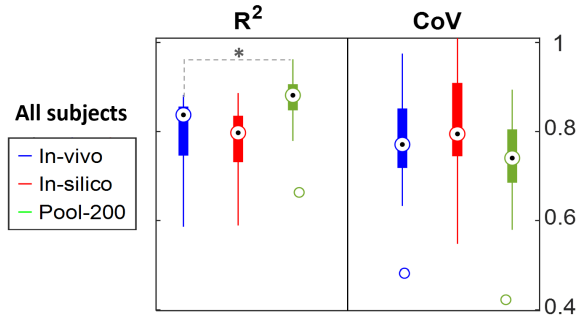

Fig. 9. Calculated R^2 and CoV for *in vivo* MNs (blue), optimized *in silico* MNs (red), and extended *in silico* pool including PDF-derived MNs (green) across all subjects and conditions. Statistical difference between *in vivo* MNs and *in silico* pool, as determined by non-parametric Friedman test, indicated by a star.

In general, we observed smaller β_Q values associated to higher discharge rates and, thus, earlier recruited (*i.e.,* smaller size) MNs. This is consistent with the size-based parameters proposed by Kohn and Abdala for different types of MNs [14]. This framework assumed the same absolute ranges of MN parameters for every subject (*i.e.,* inter-subject differences are given by the PDFs). Here, we found disctinctive PDFs for every subject (test 2, Fig. 3), with largest inter-subject variability observed in D_S. For subject 1, we observed a distinctive D_S distribution, which could be explained by the limited number of decoded MNs in comparison with other subjects. However, since our framework did not include MN-tracking to control for repeated units (*i.e.,* same MN identified in multiple contractions), we cannot discard that PDFs derive from larger MN counts may be biassed by repeated units, particularly in the lower-end of recruitment order. Future work should implement MN-tracking and assess the impact that number of decomposed MNs has on the estimation of PDFs represantive of the entire MN pool. Furthermore, future work should test wheter fixed ranges of MN parameters enable characterizing pool properties in elderly and imparied subjects, as reported adaptations in motor unit sizes and contraction speeds [41] have been suggested to be a consequence of age-related losses of larger size MNs [1], while altered MN soma sizes have been related to neuronal lesion and motor disorders [42]. Traditionally, motor unit types (*i.e.,* slow, fatigue resistant and fast fatigable) have been associated to MN soma size. Studies of human autopsies [37] reported that approximately 70 % of the motor units innervating TA are associated to small size MNs [18]. Our results showed that, for every subject, the dominant clusters C_1 and C_2 comprised together $\approx$ 70 % of the MN pool. Future work will systematically assess whether this cluster-based classification of MN parameters could be used for *in vivo* identification of distinct motor unit types.

HD-EMG decomposition revealed that the firing frequency of *in vivo* MNs increased proportionally to % MVC (Fig. 4.C). Although we did not control for coactivation of antagonist muscles (*i.e.,* MN activity may be overestimated, particularly at higher % MVCs), this is consistent with previous findings [39] suggesting that rate coding has a dominant role in the modulation of force during high speed isometric contractions. After parameter optimization, *in silico* MNs driven by *in vivo* CSI reproduced the same degree of frequency modulation (Fig. 4.C) and matched both recruitment threshold and discharge rate (Fig. 5) of *in vivo* MNs for all subjects and conditions (Fig. 6). Although these results do not validate the underlying *in silico* MN properties, especially considering the limited set of isometric contractions included in the experiment, this is the first work able to create neural-data driven models that capture subject-specific dynamics of *in vivo* MNs. Moreover, parameter ranges for optimization were derived from

the closest approximations available to *in vivo* human properties [26]. Given the technical challenge of measuring human MN properties *in vivo*, matching recruitment threshold and discharge rates is currently the only viable alternative for *in vivo* validation. Future work will aim at implementing a neuromuscular model for validation at the level of generated torque.

The resulting parameter's PDFs enabled extending the number of *in silico* MNs to complete a pool of 200 MNs (Fig. 7) while retaining the same PDFs as initially identified. Since identified PDFs of β_Q were skewed to the lower end of the distribution for every subject (Fig. 7), given the inverse relationship we found between β_Q and discharge rate, we implemented a quality-control algorithm to prevent PDF-derived *in silico* MNs from firing at discharge rates significatively larger than *in vivo* MNs. Here, we defined a tolerance of 3Hz. However, future work should systematically assess whether this threshold and rejection criteria are enough to compensate for not identified *in vivo* MNs. In comparison to the neural drive estimated from *in vivo* MNs (Fig. 8. D), this approach of driving *in silico* MN pools with trial-specific *in vivo* CSIs resulted in better estimations of force profiles as indicated by the higher R^2 achieved by the *in silico* pools (Fig. 8.C). This may be due to the availability of neural data from entire MN pools, which is not accessible via HD-EMG alone, as larger motor units (*i.e.* producing action potentials of higher amplitude) overshadow smaller units [43] and prevent identifying earlier recruited MNs. This is particularly noticeable at 30%, 40% and 50% MVC, where the *in vivo* neural drive shows large fluctuations and mismatches during the ascending/descending portions of the ramps (Fig.8.C). In contrast, additional spike trains from the *in silico* MN pool resulted in smoother neural drive estimates that follow more closely the torque profile (Fig. 8.B).Moreover, we found that R^2 of the *in silico* pool increased with % MVC. This could be explained by the larger number of recruited MNs at higher % MVCs (7). With more MNs contributing to the neural drive, the transmission of the CSI may be improved and the CoV reduced, thereby enhancing force steadiness [44]. Regardless, statistical significant improvement in R^2 was found for all subjects and conditions using *in silico* MN pools (Fig. 9). In the future, this framework could be used to complement HD-EMG decomposition for deriving mechanically consistent MN spike trains (*e.g.,* not exhibiting pauses, noise-like spikes or merging inconsistencies). However, to validate the percentage of recruited MNs from the *in silico* pool as a function of force magnitude, future work should look into the implementation of MN-specific twitch models.

As MN excitability is thought to be modulated during dynamic contractions and may vary with rate of force development [35], future work should also evaluate whether this approach for driving *in silico* pools of MNs generalize to different motor conditions. Given the challenge of predicting broader repertoires of motor tasks, future work may also look into the addition of dendritic neuromodulation to our MN models, as persistent-inward currents have been reported to play a substantial role modulating MN behavior [45].

Lastly, we emphasize that all MN pool characteristics here discussed were derived from TA, the main contributing muscle to ankle dorsi-flexion. Applying this method to other muscles may result in distinctive motor unit sizes and distributions [32]. However, although additional studies are required, we believe this same framework can be used for any muscle where the underlying neural data is available, as ranges for parameter optimization included measurements from several limb muscles [13], [26], and large inter-muscle similarities in contractile and discharge characteristics have been previously reported [32]. Future work will focus on applying this framework to different muscles and addressing the possibility of creating comprehensive subject-specific neuro-musculoskeletal models for simulating the neuro-mechanical interaction of multiple muscles.

V. Conclusion

This study demonstrated the ability of our neural-data driven framework for creating subject-specific *in silico* MN pools that enable predicting *in vivo* MN firing characteristics and muscle activation profiles throughout isometric force-tracking tasks at varying levels of amplitude. Thus, bridging the gap between current neuromechanical models and clinical practice.

Acknowledgment

The authors would like to thank Buitenweg J. and Yavuz U. for their contribution to the design of this study. They also thank Van Asseldonk E. for his advice and support.

It was brought to the authors attention that, during the editorial process, Caillet et al. published a methodology for estimating the firing behavior of complete motoneuron pools from high-density electromyography [46]. Given the affinity between their work and ours, we consider it relevant to acknowledge it here.

References

[1] M. R. Roos, C. L. Rice, and A. A. Vandervoort, "Age-related changes in motor unit function," *Muscle Nerve*, vol. 20, no. 6, pp. 679–690, 1997, doi: 10.1002/(SICI)1097-4598(199706)20:6<679::AID-MUS4>3.0.CO;2-5.

[2] G. Kamen and C. A. Knight, "Training-related adaptations in motor unit discharge rate in young and older adults," *J. Gerontology A, Biol. Sci. Med. Sci.*, vol. 59, no. 12, pp. 1334–1338, Dec. 2004, doi: 10.1093/gerona/59.12.1334.

[3] A. Del Vecchio et al., "The increase in muscle force after 4 weeks of strength training is mediated by adaptations in motor unit recruitment and rate coding," *J. Physiol.*, vol. 597, no. 7, pp. 1873–1887, Apr. 2019, doi: 10.1113/JP277250.

[4] A. Thibaut, C. Chatelle, E. Ziegler, M.-A. Bruno, S. Laureys, and O. Gosseries, "Spasticity after stroke: Physiology, assessment and treatment," *Brain Injury*, vol. 27, no. 10, pp. 1093–1105, Sep. 2013, doi: 10.3109/02699052.2013.804202.

[5] E. Lorusso, J. J. Hickman, and X. Guo, "Ion channel dysfunction and altered motoneuron excitability in ALS," *Neurological Disorders Epilepsy J.*, vol. 3, no. 2, pp. 1–13, 2019.

[6] P. Bose, R. Parmer, P. J. Reier, and F. J. Thompson, "Morphological changes of the soleus motoneuron pool in chronic midthoracic contused rats," *Experim. Neurol.*, vol. 191, no. 1, pp. 13–23, Jan. 2005, doi: 10.1016/j.expneurol.2004.08.028.

[7] A. Holobar and D. Zazula, "Gradient convolution kernel compensation applied to surface electromyograms," in *Proc. Int. Conf. Independ. Compon. Anal. Signal Separat.*, 2007, pp. 617-624.

[8] R. Merletti, A. Holobar, and D. Farina, "Analysis of motor units with high-density surface electromyography," *J. Electromyogr. Kinesiol.*, vol. 18, pp. 879–890, Dec. 2008, doi: 10.1016/j.jelekin.2008.09.002.

[9] A. Holobar, M. A. Minetto, and D. Farina, "Accurate identification of motor unit discharge patterns from high-density surface EMG and validation with a novel signal-based performance metric," *J. Neural Eng.*, vol. 11, no. 1, Feb. 2014, Art. no. 016008, doi: 10.1088/1741-2560/11/1/016008.

[10] A. D. Vecchio et al., "You are as fast as your motor neurons: Speed of recruitment and maximal discharge of motor neurons determine the maximal rate of force development in humans," *J. Physiol.*, vol. 597, no. 9, pp. 2445–2456, Mar. 2019, doi: 10.1113/JP277396.

[11] M. Sartori, U. Ş. Yavuz, and D. Farina, "In vivo neuromechanics: Decoding causal motor neuron behavior with resulting musculoskeletal function," *Sci. Rep.*, vol. 7, no. 1, pp. 1–14, Oct. 2017, doi: 10.1038/s41598-017-13766-6.

[12] A. L. Hodgkin and A. F. Huxley, "A quantitative description of membrane current and its application to conduction and excitation in nerve," *J. Physiol.*, vol. 117, pp. 500–544, Aug. 1952.

[13] R. R. L. Cisi and A. F. Kohn, "Simulation system of spinal cord motor nuclei and associated nerves and muscles, in a web-based architecture," *J. Comput. Neurosci.*, vol. 25, pp. 520–542, May 2008, doi: 10.1007/s10827-008-0092-8.

[14] L. A. Elias and A. F. Kohn, "Individual and collective properties of computationally efficient motoneuron models of types S and F with active dendrites," *Neurocomputing*, vol. 99, pp. 521–533, Jan. 2013, doi: 10.1016/j.neucom.2012.06.038.

[15] J. L. Dideriksen, F. Negro, and D. Farina, "The optimal neural strategy for a stable motor task requires a compromise between level of muscle cocontraction and synaptic gain of afferent feedback," *J. Neurophysiology*, vol. 114, no. 3, pp. 1895–1911, Sep. 2015, doi: 10.1152/jn.00247.2015.

[16] L. A. Elias, R. N. Watanabe, and A. F. Kohn, "Spinal mechanisms may provide a combination of intermittent and continuous control of human posture: Predictions from a biologically based neuromusculoskeletal model," *PLoS Comput. Biol.*, vol. 10, no. 11, Nov. 2014, Art. no. e1003944, doi: 10.1371/journal.pcbi.1003944.

[17] D. Farina, F. Negro, and J. L. Dideriksen, "The effective neural drive to muscles is the common synaptic input to motor neurons," *J. Physiol.*, vol. 592, no. 16, pp. 3427–3441, Aug. 2014, doi: 10.1113/jphysiol.2014.273581.

[18] J. E. Zengel, S. A. Reid, G. W. Sypert, and J. B. Munson, "Membrane electrical properties and prediction of motor-unit type of medial gastrocnemius motoneurons in the cat," *J. Neurophysiology*, vol. 53, no. 5, pp. 1323–1344, May 1985, doi: 10.1152/jn.1985.53.5.1323.

[19] S. Cullheim, J. W. Fleshman, L. L. Glenn, and R. E. Burke, "Membrane area and dendritic structure in type-identified triceps surae alpha motoneurons," *J. Comparative Neurol.*, vol. 255, no. 1, pp. 68–81, Jan. 1987, doi: 10.1002/cne.902550106.

[20] W. Van Geit, E. De Schutter, and P. Achard, "Automated neuron model optimization techniques: A review," *Biol. Cybern.*, vol. 99, nos. 4–5, pp. 241–251, Nov. 2008, doi: 10.1007/s00422-008-0257-6.

[21] M. C. Vanier and J. M. Bower, "A comparative survey of automated parameter-search methods for compartmental neural models," *J. Comput. Neurosci.*, vol. 7, no. 2, pp. 149–171, Sep. 1999, doi: 10.1023/A:1008972005316.

[22] S. Druckmann, "A novel multiple objective optimization framework for constraining conductance-based neuron models by experimental data," *Frontiers Neurosci.*, vol. 1, no. 1, pp. 7–18, Nov. 2007, doi: 10.3389/neuro.01.1.1.001.2007.

[23] S. Masoli, M. F. Rizza, M. Sgritta, W. Van Geit, F. Schürmann, and E. D'Angelo, "Single neuron optimization as a basis for accurate biophysical modeling: The case of cerebellar granule cells," *Frontiers Cellular Neurosci.*, vol. 11, pp. 1–14, Mar. 2017, doi: 10.3389/fncel.2017.00071.

[24] A. Gogeascoechea et al., "Interfacing with alpha motor neurons in spinal cord injury patients receiving trans-spinal electrical stimulation," *Frontiers Neurol.*, vol. 11, pp. 1–12, Jun. 2020, doi: 10.3389/fneur.2020.00493.

[25] A. Destexhe, "Conductance-based integrate-and-fire models," *Neural Comput.*, vol. 9, no. 3, pp. 503–514, Mar. 1997, doi: 10.1162/neco.1997.9.3.503.

[26] A. H. Caillet, A. T. Phillips, D. Farina, and L. Modenese, "Mathematical relationships between spinal motoneuron properties," *eLife*, vol. 11, pp. 1–27, Jul. 2022, doi: 10.7554/eLife.76489.

[27] R. O. Kobayashi, A. Gogeascoechea, J. Buitenweg, U. Yavuz, and M. Sartori, "Optimization framework for the model-based estimation of in vivo α-motoneuron properties in the intact human," in *Proc. 43rd Annu. Int. Conf. IEEE Eng. Med. Biol. Soc. (EMBC)*, Nov. 2021, pp. 6133–6136, doi: 10.1109/EMBC46164.2021.9630260.

[28] Z. Wang and G. P. Rangaiah, "Application and analysis of methods for selecting an optimal solution from the Pareto-optimal front obtained by multiobjective optimization," *Ind. Eng. Chem. Res.*, vol. 56, no. 2, pp. 560–574, Dec. 2016, doi: 10.1021/acs.iecr.6b03453.

[29] G. Guariso and M. Sangiorgio, "Improving the performance of multiobjective genetic algorithms: An elitism-based approach," *Information*, vol. 11, no. 12, p. 587, Dec. 2020, doi: 10.3390/info11120587.

[30] C. Clopath, R. Jolivet, A. Rauch, H.-R. Lüscher, and W. Gerstner, "Predicting neuronal activity with simple models of the threshold type: Adaptive exponential integrate-and-fire model with two compartments," *Neurocomputing*, vol. 70, nos. 10–12, pp. 1668–1673, Jun. 2007, doi: 10.1016/j.neucom.2006.10.047.

[31] M. C. Jones, "Simple boundary correction for kernel density estimation," *Statist. Comput.*, vol. 3, no. 3, pp. 135–146, Sep. 1993, doi: 10.1007/BF00147776.

[32] J. Duchateau, R. M. Enoka, and J. Duchateau, "Distribution of motor unit properties across human muscles," *J. Appl. Physiol.*, vol. 132, no. 1, pp. 1–13, 2021, doi: 10.1152/japplphysiol.00290.2021.

[33] R. M. Enoka and A. J. Fuglevand, "Motor unit physiology: Some unresolved issues," *Muscle Nerve*, vol. 24, no. 1, pp. 4–17, 2001, doi: 10.1002/1097-4598(200101)24:1<4::AID-MUS13>3.0.CO;2-F.

[34] D. Arthur and S. Vassilvirskii, "K-means++: The advantages of careful seeding," in *Proc. 18th Annu. ACM-SIAM Symp. Discrete Algorithms*, 2007, pp. 1027–1035.

[35] J. E. Desmedt and E. Godaux, "Ballistic contractions in man: Characteristic recruitment pattern of single motor units of the tibialis anterior muscle," *J. Physiol.*, vol. 264, no. 3, pp. 673–693, 1977, doi: 10.1113/jphysiol.1977.sp011689.

[36] M. V. Cutsem, P. Feiereisen, J. Duchateau, and K. Hainaut, "Mechanical properties and behaviour of motor units in the tibialis anterior during voluntary contractions," *Can. J. Appl. Physiol.*, vol. 22, no. 6, pp. 585–597, Nov. 1997, doi: 10.1139/h97-038.

[37] M. A. Johnson, J. Polgar, D. Weightman, and D. Appleton, "Data on the distribution of fibre types in thirty-six human muscles. An autopsy study," *J. Neurol. Sci.*, vol. 18, pp. 111–129, Jan. 1973, doi: 10.1016/0022-510X(73)90023-3.

[38] D. Kernell, "High-frequency repetitive firing of cat lumbosacral motoneurones stimulated by long-lasting injected currents," *Acta Physiologica Scandinavica*, vol. 65, nos. 1–2, pp. 74–86, Sep. 1965, doi: 10.1111/j.1748-1716.1965.tb04251.x.

[39] R. M. Enoka and J. Duchateau, "Rate coding and the control of muscle force," *Cold Spring Harbor Perspect. Med.*, vol. 7, no. 10, pp. 1–12, 2017, doi: 10.1101/cshperspect.a029702.

[40] E. Hennema, G. Somjen, and D. O. Carpenter, "Functional significance of cell size in spinal motoneurons," *J. Neurophysiol.*, vol. 28, no. 3, pp. 560–580, 1965, doi: 10.1152/jn.1965.28.3.560.

[41] T. J. Doherty and W. F. Brown, "Age-related changes in the twitch contractile properties of human thenar motor units," *J. Appl. Physiol.*, vol. 82, no. 1, pp. 93–101, Jan. 1997, doi: 10.1152/jappl.1997.82.1.93.

[42] S. S. Dukkipati, T. L. Garrett, and S. M. Elbasiouny, "The vulnerability of spinal motoneurons and soma size plasticity in a mouse model of amyotrophic lateral sclerosis," *J. Physiol.*, vol. 596, no. 9, pp. 1723–1745, 2018, doi: 10.1113/JP275498.

[43] A. Gogeascoechea, R. O. Kobayashi, U. S. Yavuz, and M. Sartori, "Identification of motor unit twitch properties in the intact human in vivo," in *Proc. 43rd Annu. Int. Conf. IEEE Eng. Med. Biol. Soc. (EMBC)*, Nov. 2021, pp. 6310–6313, doi: 10.1109/EMBC46164.2021.9630328.

[44] F. Negro, A. Holobar, and D. Farina, "Fluctuations in isometric muscle force can be described by one linear projection of low-frequency components of motor unit discharge rates," *J. Physiol.*, vol. 587, no. 24, pp. 5925–5938, Dec. 2009, doi: 10.1113/jphysiol.2009.178509.

[45] C. J. Heckman, M. Johnson, C. Mottram, and J. Schuster, "Persistent inward currents in spinal motoneurons and their influence on human motoneuron firing patterns," *Neuroscientist*, vol. 14, no. 3, pp. 264–275, Jun. 2008, doi: 10.1177/1073858408314986.

[46] A. H. Caillet, A. T. M. Phillips, D. Farina, and L. Modenese, "Estimation of the firing behaviour of a complete motoneuron pool by combining electromyography signal decomposition and realistic motoneuron modelling," *PLoS Comput. Biol.*, vol. 18, no. 9, 2022, Art. no. e1010556, doi: 10.1371/journal.pcbi.1010556.